JOURNAL OF AIRCRAFT
Vol. 39, No. 1, January–February 2002

Numerical Investigations of Dynamic Stall Active Control for Incompressible and Compressible Flows

John A. Ekaterinaris*
Foundation for Research and Technology Hellas (FO.R.T.H.), 71110 Heraklion, Greece

Numerical investigations of active flow control, which can offer significant improvements to aircraft, helicopter, and wind-turbine rotor performance by suppressing detrimental effects of separated flow and dynamic stall, are presented. Simulations of pulsating jet flow control applied on airfoils executing oscillatory motion are carried out to demonstrate improvements in dynamic performance obtained for high-Reynolds-number turbulent flow dynamic stall. Currently available efficient and accurate numerical methods for the Navier–Stokes equations and advanced turbulence models are used for the prediction of the complex, unsteady flowfields. Both incompressible and compressible flow conditions are considered. It is found that pulsating jet flow control can significantly reduce the adverse effects of dynamic stall. The effect of the jet location on dynamic stall characteristics is investigated.

I. Introduction

ACTIVE and passive flow control of separated flow over cylinders and airfoils at high incidences or airfoils executing dynamic motion has been a subject of experimental and theoretical investigation for the past decades. Passive and active flow controls concepts have been tested in numerous experimental investigations.[1–7] It has been demonstrated that its application can yield significant improvements in aerodynamic performance. For example, in Ref. 1 flow separation over airfoils at high incidence has been successfully suppressed by high-frequency transverse velocity fluctuations generated by acoustic excitations. More recently, control of separated flows with pulsating jets[2,3,8,9] yielded very encouraging results. Advances in "smart," compact flow actuation devices, such as synthetic jets,[10] opened new horizons in flow actuation and can lead to significant improvements in aerodynamic performance of existing configurations. These devices can be used to control flow separation, to enhance existing capabilities of control surfaces, and to provide additional maneuverability by either replacing or enhancing the effectiveness of traditional control surfaces, such as trailing-edge flaps. In contrast to older techniques for manipulation of flow separation,[11] such as steady blowing/suction,[4] the new active flow actuation methods[8,10] have the advantage that they require significantly less power input and introduce smaller design complexities. For example, the innovative method of flow control with synthetic jets requires only electric power and produces a high-frequency pulsating jet with zero net mass input. Pneumatic flow control with pulsating jets, on the other hand,[2,3] can yield large improvements in performance with a small jet output rate.

In many practical applications, such as wind turbines and helicopter rotors, as well as turbomachinary, rapid pitching blade motions generate dynamic stall. Dynamic stall is a limiting factor for more widespread use of helicopters in both military and civilian applications and can cause extreme loading to wind-turbine rotors and turbomachinary blades. Because of the negative impact of dynamic stall, basic research (see Ref. 12 and references therein) has focused on the understanding of the basic mechanisms causing its occurrence. Developing the ability to numerically predict and devising means to prevent, control, or possibly eliminate, dynamic stall is important to efforts toward improving aerodynamic performance of rotating machinery and maneuvering aircraft. Dynamic stall reduces the maximum cruise speed of helicopters because it generates excessive loads on the rotor and flight controls. Passive[7] and active[5] flow controls can be used on rotors to reduce or possibly completely eliminate the detrimental effects of dynamic stall.

Alterations of the flow at the leading-edge region of thin airfoils are most effective in controlling dynamic stall. Therefore, several leading-edge boundary-layer control methods have been employed in rotorcraft applications. These methods include steady blowing or suction,[4] unsteady blowing,[2–5] and boundary-layer transition.[6] It has been demonstrated[2,5] that oscillatory blowing is more effective than steady blowing in delaying dynamic stall. This flow control improves dynamic airfoil performance by reducing dynamic stall hysteresis effects significantly and by eliminating large excursions in lift, drag, and pitching moment during the oscillation cycle. Another category of dynamic stall control methods, which have been investigated, are based on modifications of the blade leading-edge geometry. Examples include passive controls, such as leading-edge slats,[7] active airfoil geometry modifications, such as nose drooping,[13] and dynamically deforming leading-edge radius.[6]

Numerical prediction of the beneficial effects of flow control reported in experimental studies was the subject of recent investigation by Wu et al.,[14] where flow control was simulated by a pulsating jet, which was located at $s_J = x/c = 0.025$, and blowing was prescribed in the normal to the airfoil surface direction. It was found that lift increase in the poststall regime can be achieved as was reported in the experiments. The effectiveness of a pulsating jet located at the leading edge $s_J = 0$ chord of a NACA-0015 airfoil to control static stall was also investigated in the numerical investigation of Ref. 15. Hassan and JanakiRam[16] and Hassan[17] investigated the effectiveness of a jet located at $s_J = 0.13$ chord to control flow separation using Navier–Stokes methods and reported that a high jet momentum is needed to obtain a significant lift increase. In the numerical study of Ref. 18, simulations of steady and pulsating jet flow controls were shown. McCormick[9] developed a new concept for boundary-layer separation control, the so-called directed synthetic jet. The blowing slot of this jet is curved in the downstream direction. The jet energizes the boundary layer and makes it, in the time average, more resistant to separation. Calculated lift coefficients of the directed synthetic jet for airfoil static stall control[9] were in agreement with the experiment. In the present investigation the jet exit velocity is also prescribed in a direction almost tangential to the airfoil surface.

Effective control of dynamic stall over oscillating airfoils was achieved with pulsating jets.[5] In contrast to the synthetic jets,[8] pulsating jets apply unsteady bleeding or blowing using more hardware

Presented as Paper 2000-4333 at the Applied Aerodynamics Conference, received 7 September 2000; revision received 20 August 2001; accepted for publication 24 September 2001.

*Senior Research Scientist, Institute of Applied and Computational Mathematics, P.O. Box 1527; ekaterin@iacm.forth.gr. Associate Fellow AIAA.

intensive mechanisms. They require external pumps and piping in order to generate the pressure oscillations necessary for the zero-mass-flux flow control. More recently the effectiveness of pulsating jets was demonstrated for control of compressible, high-Reynolds-number separated flows.[3] Synthetic jet flow control devices,[8] on the other hand, use membranes or springboards, which are driven at resonance piezoelectrically or mechanically by motors and enhance the momentum of boundary layer by zero mass vortical flow. Synthetic jets were successfully used to control flow separation of low-Reynolds-number incompressible flows.[8] Further demonstration of the ability of pneumatic flow controls to improve aerodynamic performance of high-Reynolds-number incompressible and compressible unsteady flows and dynamic stall is needed. To date, there are no analytical tools available to determine the range of parameters, such as jet location and speed or momentum coefficient and pulsation frequency, for which flow control methods are most effective. As a result, for every new airfoil shape at fixed incidences or for pitching airfoils with different unsteady parameters, such as oscillation amplitude or rate, the flow actuation parameters are determined heuristically.

Numerical simulation of active pneumatic flow control over airfoils with synthetic jet actuators as it was done in Ref. 8 for simple flows is computationally intensive because it requires detailed simulation of the synthetic jet device including the cavity and the exit slot. The flow scales that must be resolved in the synthetic jet actuator and the vicinity of the exit slot are small compared with the airfoil boundary-layer scale. A well-resolved simulation of the synthetic jet requires a large number of grid points and incorporation of the cavity actuation mechanism, such as an oscillating membrane at the end of the cavity. Simulation of pulsating jet flow control for high-Reynolds-number ($Re_c > 10^6$) airfoil flows, on the other hand, can be accomplished either by time-accurate simulation of the Reynolds-averaged Navier–Stokes (RANS) equations or by large eddy simulations (LES). LES computations of the time-dependent flowfield generated by the synthetic jet are beyond the available computing resources.

In the present investigation pulsating jet flow control[5] is applied on oscillating airfoils as it was done in Refs. 15–17 for stationary airfoils. The jet flow is imposed as a boundary condition on the airfoil surface. Time-accurate solutions of the RANS equations are used for both flows at fixed incidence and for flows over oscillating airfoils. A schematic of a pulsating jet located on the suction side at $x/c = s_J$ chord distance from the leading edge exiting almost tangent to the airfoil surface at an angle $\theta_{\rm jet}$ is shown in Fig. 1. An increased grid resolution is used in the region where the pulsating jet is considered. For leading-edge pulsating jets the airfoil shape is slightly altered in order to include a jet blowing almost tangentially to the airfoil surface. The detail of the grid used for numerical simulation of flow control with a leading-edge pulsating jet is shown in Fig. 2.

The effectiveness of pulsating flow controls is evaluated for fully turbulent flow conditions and for incompressible and compressible flow speeds by performing RANS numerical simulations with advanced turbulence models. The computational tools that are used for the numerical simulations have been extensively validated for unsteady flow computations and dynamic stall[19–22] by comparison with experimental data.

It was demonstrated in the experiments[5] that the important parameters for airfoil flow control with pulsating jets are the reduced excitation frequency $F^+ = f_J c / U_\infty$, where c is the airfoil chord; f_J is the jet pulsation frequency; the oscillatory blowing momentum coefficient is $C_\mu = \langle J \rangle / cq$, where $q = 0.5 \rho U_\infty^2$; $\langle J \rangle$ is the oscillatory momentum, $\langle J \rangle = \rho V_J^2 H_J$; H_J is the jet slot width; and V_J is the jet velocity oscillation amplitude. For the numerical simulations in order to ensure that effective flow control is obtained, we use high values of jet pulsation frequency $F^+ > 1$ and momentum coefficient $C_\mu > 0.1\%$. Dynamic stall developing over a NACA-0015 airfoil for low pitch-up rate, $k = \pi f_a c / U_\infty = 0.05$, is computed first. The numerical simulations are fully turbulent, and, except for the Reynolds number, the other flow parameters match the parameters of the measurements by Greenblatt et al.[2] and Greenblatt and Wygnanski.[5] Therefore, dynamic stall measurements by Piziali,[23] performed for high-Reynolds-number tripped flow, are also used to validate the computations and to demonstrate the effect of flow control on hysteresis loops. Numerical simulations of pulsating jet flow control where the location of the jet is a free parameter are carried out next. The objective of this investigation is to demonstrate that numerical solutions can be used to perform a sensitivity analysis of flow control parameters. As an example, the jet location for the most effective control of two-dimensional airfoil dynamic stall is identified.

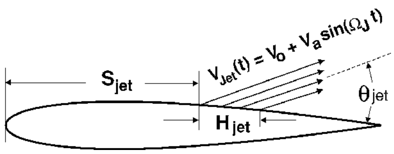

Fig. 1 Schematic of slat for pulsating jet at the upper surface.

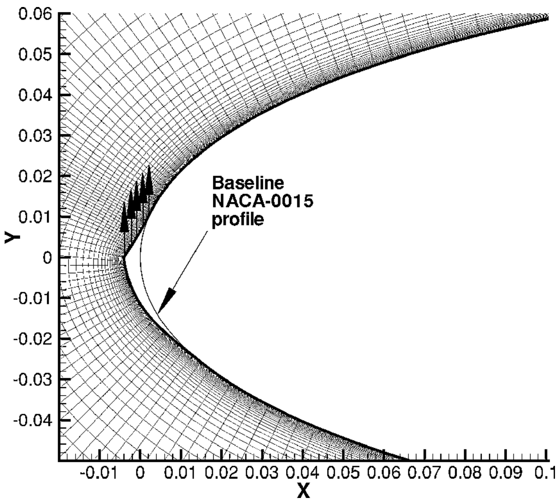

Fig. 2 Leading-edge grid detail and schematic of pulsating jet at the leading edge.

II. Governing Equations

Pulsating jet flow control simulations require time-accurate solutions of the governing equations. The governing equations used for the numerical simulations of both incompressible and compressible subsonic flows are shown in the next sections. In both cases the flow was assumed fully turbulent, and the eddy viscosity was obtained from the one-equation turbulence model.

A. Incompressible Flow Equations

In many industrial applications the performance of components, such as flows over hydrofoils and wind-turbine blades, is affected by dynamic stall developing at low speeds $M_\infty < 0.1$, where the flow is practically incompressible. The primary problem with time-accurate solutions of the incompressible flow equations is the difficulty of coupling changes in the velocity field with changes in the pressure field while satisfying the continuity equation. The artificial compressibility or pseudocompressibility method is often used to overcome these difficulties. This method was initially introduced by Chorin[24] for the solution of steady-state incompressible flows, and it was subsequently extended[25] to time-accurate incompressible flow solutions. The artificial compressibility formulation can be utilized for the solution of unsteady flows when a pseudotime derivative of pressure is added to the continuity equation. This term directly couples the pressure with velocity and allows the equations to advance in physical time by iterating until a divergence-free velocity field is obtained at the new physical time level.

The artificial compressibility or pseudocompressibility formulation is obtained from the original incompressible flow equations by introducing an additional time derivative of pressure to the continuity equation as

$$\frac{\partial p}{\partial \tau} = -\beta \nabla \cdot \hat{\boldsymbol{U}} = -\beta \left[\frac{\partial}{\partial \xi}\left(\frac{U}{J}\right) + \frac{\partial}{\partial \eta}\left(\frac{V}{J}\right) \right] \tag{1}$$

Addition of this fictitious pressure derivative enables full coupling of the continuity with the momentum equations and significantly facilitates the numerical solution. In Eq. (1) τ does not represent physical time; therefore, in the momentum equation t is replaced by τ, and the pseudocompressible form of the governing equations is

$$\frac{\partial \hat{\boldsymbol{Q}}}{\partial \tau} + \frac{\partial \hat{\boldsymbol{F}}}{\partial \xi} + \frac{\partial \hat{\boldsymbol{G}}}{\partial \eta} = \frac{1}{Re}(\hat{\boldsymbol{F}}_v + \hat{\boldsymbol{G}}_v) \tag{2}$$

where $\hat{\boldsymbol{Q}} = [p, u, v]^T/J$ is the solution variable vector and $\hat{\boldsymbol{F}}$, $\hat{\boldsymbol{G}}$, and $\hat{\boldsymbol{F}}_v$, $\hat{\boldsymbol{G}}_v$ are the inviscid and viscous flux vectors, respectively.

In these equations τ is referred to as pseudotime, which can be considered as a time iteration parameter. Steady-state incompressible solutions are obtained with the artificial compressibility method by time marching as in the compressible case. The numerical methods for the solution of the pseudocompressible equations are very similar to the methods used for the solutions of the compressible flow equations.[26,27] At convergence, however, the time derivative of pressure, and consequently the divergence of the velocity, approach zero. The parameter β, which is referred to as the artificial compressibility or pseudocompressibility parameter, usually takes a value between 1 and 5, but larger values might be required for solutions on highly stretched grids. Time-accurate solutions of unsteady flows with the pseudocompressibility formulation with implicit schemes are obtained using dual time stepping[26,27] as shown in the next section.

B. Compressible Flow Equations

In the compressible flow simulations the thin-layer approximation of the Navier–Stokes equations is used. These equations in curvilinear, body-fitted coordinates (ξ, η) are

$$\frac{\partial \boldsymbol{Q}}{\partial t} + \frac{\partial \boldsymbol{F}(\boldsymbol{q})}{\partial \xi} + \frac{\partial \boldsymbol{G}(\boldsymbol{q})}{\partial \eta} = \frac{\partial \boldsymbol{G}_v(\boldsymbol{q})}{\partial \eta} \tag{3}$$

where $\boldsymbol{Q} = J^{-1}[\rho, \rho u, \rho v, e]^T = \boldsymbol{q}/J$ is the solution vector, J is the Jacobian of the coordinate transformation, and $\boldsymbol{F}$ and $\boldsymbol{G}$ are the flux vectors in curvilinear coordinates. For example, $\boldsymbol{F} = J^{-1}[\rho U, \rho u U + \xi_x p, \rho v U + \xi_y p, (e+p)U - \xi_t p]^T$, where U is the contravariant velocity component $U = \xi_x u + \xi_y v + \xi_t$, and u, v are the Cartesian velocity components. The pressure p for a calorically perfect gas is related to the other variables through the equation of state as $p = (\gamma - 1)[e - 0.5\rho(u^2 + v^2)]$.

III. Numerical Implementation

Simulations of the time-dependent flowfields generated by the pulsating jets are obtained on C-type meshes. At the location slot for the pulsating jet, an almost uniform grid resolution of approximately 20 points for the slot width H_h (see Figs. 1 and 2) is used. Grid points are clustered in the streamwise direction upstream and downstream of the jet slot location. In the direction normal to the airfoil surface, a sufficient number of grid points is used to provide the resolution needed for the high-Reynolds-number turbulent flow. The detail of the grid used for a jet at the leading edge $s = 0.0$ is shown in Fig. 2.

For both incompressible, Eq. (2), and compressible, Eq. (3), flow formulations space discretization of the convective fluxes is performed using upwinding and Roe's approximate Riemann solver.[28] Third-order-accurate, upwind-biased formulas are used to evaluate the convective flux derivatives. The viscous terms are computed using second-order-accurate central differences. The eddy viscosity is computed using the one-equation turbulence model of Spalart and Allmaras.[29] Essential details of the numerical algorithms are given in the following sections.

A. Incompressible Formulation

A three-dimensional version of the incompressible flow solver was used before to obtain time-accurate solution over a rotating blade.[26] Using the same formulation, two-dimensional, time-accurate solutions needed for the present investigation are obtained by using the following second-order-accurate, three-time level formulas to evaluate the time derivatives in the momentum equations

$$\frac{3\boldsymbol{u}^{n+1} - 4\boldsymbol{u}^n + \boldsymbol{u}^{n-1}}{2\Delta t} = -R^{n+1} \tag{4}$$

where R represents the right-hand-side terms $R = (\hat{F} - \hat{F}_v)_\xi + (\hat{G} - \hat{G}_v)_\eta$ and $\Delta Q = Q^{m+1} - Q^m$.

Equation (4) is solved for a divergence-free velocity field at the $(n+1)$ time level by introducing a pseudotime level, which is denoted by the superscript m in the following artificial compressibility relation:

$$\frac{\partial p}{\partial \tau} = -\beta \nabla \cdot \boldsymbol{u}^{n+1,m+1} \tag{5}$$

An iterative solution of this equation is performed so that $\boldsymbol{u}^{n+1,m+1}$ approaches $\boldsymbol{u}^{n+1}$ as $\nabla \cdot \boldsymbol{u}^{n+1,m+1}$ approaches zero.

The delta form of the linearized, unfactored, implicit algorithm, for both steady-state and time-accurate solutions is given by

$$\left[\frac{I_{\text{tr}}}{J} + \left(\frac{\partial R}{\partial Q}\right)^{n+1,m} \right] \times (Q^{n+1,m+1} - Q^{n+1,m})$$

$$= -R^{n+1,m} - \frac{I_m}{\Delta t}(1.5Q^{n+1,m} - 2Q^n + 0.5Q^{n-1}) \tag{6}$$

where $I_{\text{tr}} = \text{diag}[\Delta t/\Delta\tau, 1.5, 1.5]/\Delta t$ and $I_m = \text{diag}[0, 1, 1]$. The algorithm for steady-state solutions is obtained from Eq. (6) when the internal iteration index m is dropped, and only the first term R is retained on the right-hand side.

B. Compressible Formulation

In the past years several numerical investigations of dynamic stall of simple airfoils[19] and pitching blades[20] have been performed with the code we use to simulate compressible flows. The computed results for dynamic stall cases were in agreement with measurements, and they are summarized in the review of Ref. 12. The computer code solves the time-dependent compressible flow equations in curvilinear body-fitted coordinates. It has been developed for the numerical investigation of dynamic stall flows[19,20] and has also been tested for other unsteady aerodynamic applications.[21,22] It performs implicit time marching using an alternating-direction-implicit scheme.

IV. Results

Flow control with pulsating jets for stationary NACA-0015 airfoils was performed first as an additional validation test of the computational approach. For incompressible flow a solution with flow control at the leading edge was obtained at $\alpha = 22$ deg, $Re_c = 1.2 \times 10^6$ for a NACA-0015 airfoil. The same values of control parameters, $k_j = F^+ = 0.58$, $C_\mu = 0.0003$ of Ref. 15, were used. The computed load variation was in agreement with the low-Mach-number ($M = 0.15$) computations of Ravindran.[15] For compressible flow, the computed load variation for flow cotrol with transverse jets at $x/c \approx 0.1$ was in good agreement with the results of Hassan and Munts.[30]

Numerical simulations of flows over an oscillating NACA-0015 airfoil with pulsating jet flow control for compressible and incompressible flows were carried out next. Different locations for the pulsating jet are considered. A schematic of the pulsating jet is shown in Fig. 1, and an example of the numerical mesh used for simulation of flow control with leading-edge pulsating jet is shown in Fig. 2. It was found that the direction of the jet exit velocity with respect to the airfoil surface (denoted as θ_{jet} in Fig. 1) is an important flow control parameter. Numerical experiments demonstrated that for the poststall regime no effective flow control of dynamic stall can be achieved for a jet exiting normal to the airfoil surface. In addition, the computed loads showed a large variation at the jet pulsation frequency. Using a smaller, near-tanget exit angle, $\theta_{\mathrm{jet}} = 30$ deg, as in static stall computations of Refs. 9 and 30, it was found that dynamic stall was suppressed, but a fairly large oscillation amplitude of the computed loads at the jet pulsation frequency was also obtained. A further reduction of the jet exit angle to $\theta_{\mathrm{jet}} = 5$ deg reduced more of these oscillations. Therefore, $\theta_{\mathrm{jet}} = 5$ deg is used in the simulations. The jet exit speed V_{jet}, which is nondimensionalized with the freestream, varies as $V(t)_{\mathrm{jet}} = V_0 + V_a \cos(\Omega_J t)$, where V_0 is the mean and V_a is the amplitude. For a vanishing mean component $V_0 = 0.0$, a zero net mass flux jet is obtained. The zero net mass flux jet is used in the simulations.

A. Baseline Airfoil Computations

Compressible flow simulations are carried out at relatively low freestream speed $M = 0.3$, which matches the freestream speed of the dynamic stall measurements in Ref. 23. The Reynolds number for all cases is fixed at $Re_c = 5.0 \times 10^6$, and the flow is assumed fully turbulent. This Reynolds number is representative of in-flight flow conditions but higher than the Reynolds number reported in measurements of both Greenblatt et al.[2] and Greenblatt and Wygnanski[5] and Piziali.[23] In the first case[2,5] the experimental Reynolds number is $0.3 \times 10^6 < Re_c < 0.9 \times 10^6$, and transitional flow effects are important, whereas in the second case the flow is tripped and the fully turbulent flow assumption is a good approximation. Comparisons with the experiment of the computed load hysteresis loops obtained for deep stall for both incompressible and compressible flow and oscillatory motion with $\alpha(t) = 13\ \mathrm{deg} + 5\sin(\omega_a t)$, $k = 0.05$ are shown in Fig. 3. The arrows indicate the loop direction from upstroke to downstroke. A C-type 381×91 point grid with 301 points on the airfoil surface was used for the computation. The computations were performed for Reynolds number $Re_c = 5.0 \times 10^6$, and the flow was assumed fully turbulent. Comparisons are shown with the incompressible flow data of Ref. 5 for measurements obtained at $Re_c = 0.3 \times 10^6$ and the compressible flow measurements of Ref. 23 where the freestream speed was the same as in the computation $(M_\infty = 0.3)$ and the flow was tripped. The flow of Ref. 23 at $Re_c = 2.0 \times 10^6$ is expected to be fully turbulent as the computatios for $Re_c = 5.0 \times 10^6$.

Time periodic response is obtained after two cycles, and the load hysteresis loops of Fig. 3 correspond to the second computation cycle. The incompressible flow experiment[5] was performed at low Reynolds number $(Re_c = 0.3 \times 10^6)$, and transitional flow behavior might be responsible for the development of dynamic stall at a lower angle of incidence during the cycle. Fully turbulent compressible flow computations for the same Reynolds number as the experiment $Re_c = 2.0 \times 10^6$ have shown very little difference from the results obtained at $Re_c = 5.0 \times 10.^6$ In the compressible flow computations it was found that during the upstroke at approximately $\alpha = 14$ deg a supersonic flow region is developed close to the leading edge. As the angle of incidence is further increased, a weak shock is generated. This shock does not cause, however, flow separation. Both the incompressible and the compressible computations are in reasonably good agreement with the turbulent flow measurements of Ref. 23. However, they show only qualitative agreement with the low-Reynolds-number measurements of Ref. 5. In the following comparisons only the compressible flow measurements are retained to indicate the beneficial effects of flow control.

Simulations of dynamic stall control with pulsating jets were obtained for nondimensional jet reduced frequencies $k_j = F^+ = 6.3$ and $F^+ = 3.1$ and blowing rates of $C_\mu = 0.5$ and 2.5%. As already stated, the a high value of the jet reduced frequency was chosen to ensure effective flow control and keep the oscillation of the loads at the jet pulsation frequency at low levels. For this choice of flow control parameters, flow control simulations with pulsating jets were carried out for stationary airfoil at incidences above the static stall angle $\alpha = 16$ and 18 deg. The numerical solution was carried out for a large number of forcing cycles until all of the startup transients were removed. The mean value of the computed, time-varying lift coefficient at these fixed incidences exceeded the computed values without the control. Similarly for the dynamic stall flow control computation the flow with the pulsating jet on was computed at the lower angle of incidence until time periodicity was reached. The oscillatory motion of the airfoil with the flow control on was computed for two oscillation cycles. The computed loads reached time periodicity, and the results of the second cycle were identical to the results of the third cycle. In the following section computed results

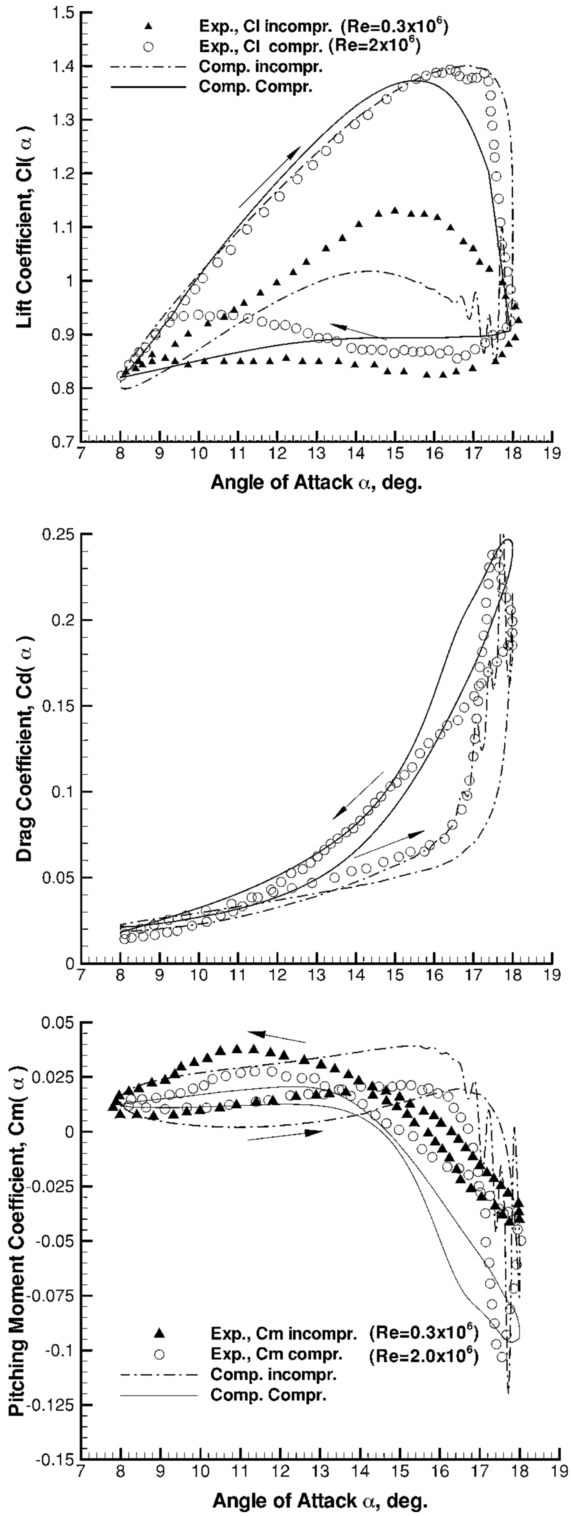

Fig. 3 Comparison of the computed loads for $Re_c = 5.0 \times 10^6$ (assumed fully turbulent), $\alpha(t) = 13\ \mathrm{deg} + 5\sin(\omega_a t)$, $k_a = 0.05$, and the measured loads of Ref. 5 for $Re_c = 0.3 \times 10^6$ and Ref. 23 for $Re_c = 2.0 \times 10^6$ and tripped flow.

are presented first for incompressible and then for compressible flow.

B. Incompressible Flow Control

The implicit time-integration scheme requires subiterations in order to ensure that incompressibility is enforced. The implicit solver time step, however, is not limited by Courant–Friedrichs–Lewy numerical stability. High pulsation frequencies of the pneumatic flow control, on the other hand, introduce small time scales, which need to be sufficiently resolved during the time-accurate computations. Therefore, the physical time step in the computations of incompressible flowfields for both stationary and harmonically oscillating airfoils was adjusted so that one jet pulsation period is resolved with at least 40 time steps.

The computed load hysteresis loop for flow control obtained by a leading-edge pulsating jet (see Fig. 2) with $F^+ = 6.3$ and $C_\mu = 0.5\%$ is compared in Fig. 4 with the high-Reynolds-number measurements of Ref. 23 and the baseline airfoil computation. The leading-edge pulsating jet reduces the dynamic stall hysteresis effects and causes a more rapid flow reattachment during the downstroke. A significant reduction of the maximum excursions of the drag $Cd(\alpha)$ and pitching moment $Cm(\alpha)$ coefficients is observed. The small-scale

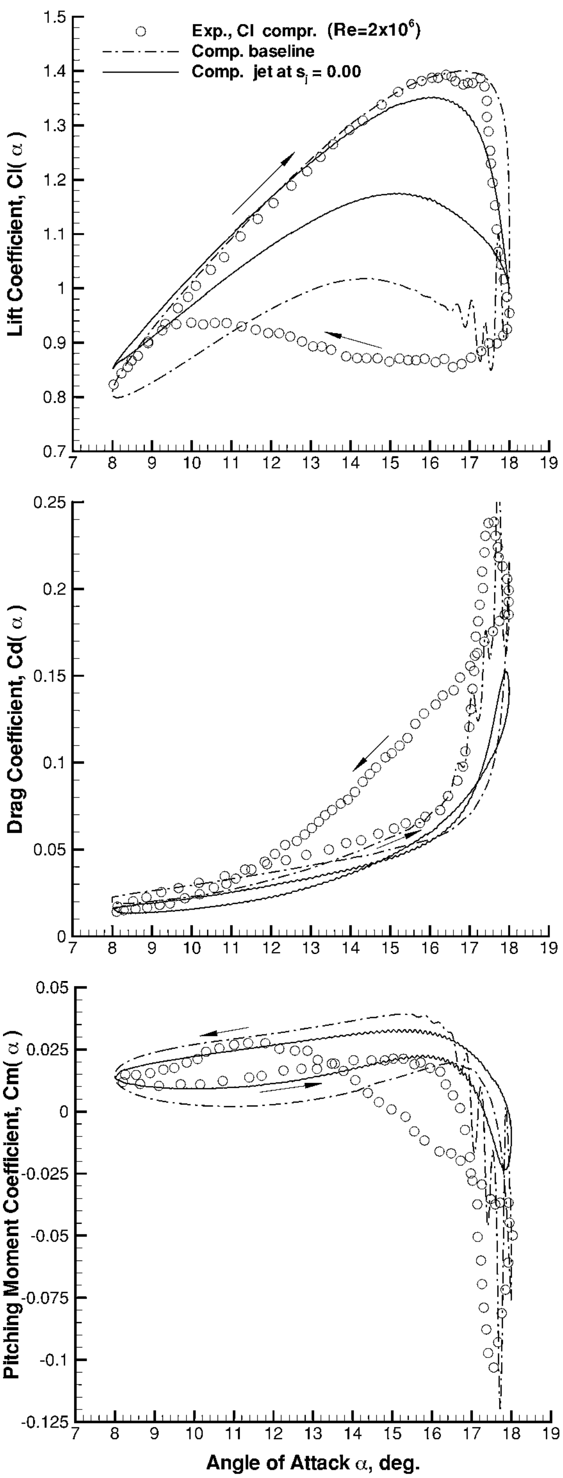

Fig. 4 Effect of pulsating jet flow control on the computed loads; $Re_c = 5.0 \times 10^6$ (fully turbulent incompressible), $\alpha(t) = 13$ deg + 5 $\sin(\omega_a t)$, $k_a = 0.05$ and $s_J = 0.0$, $F_J^+ = 6.3$, $C_\mu = 0.5\%$.

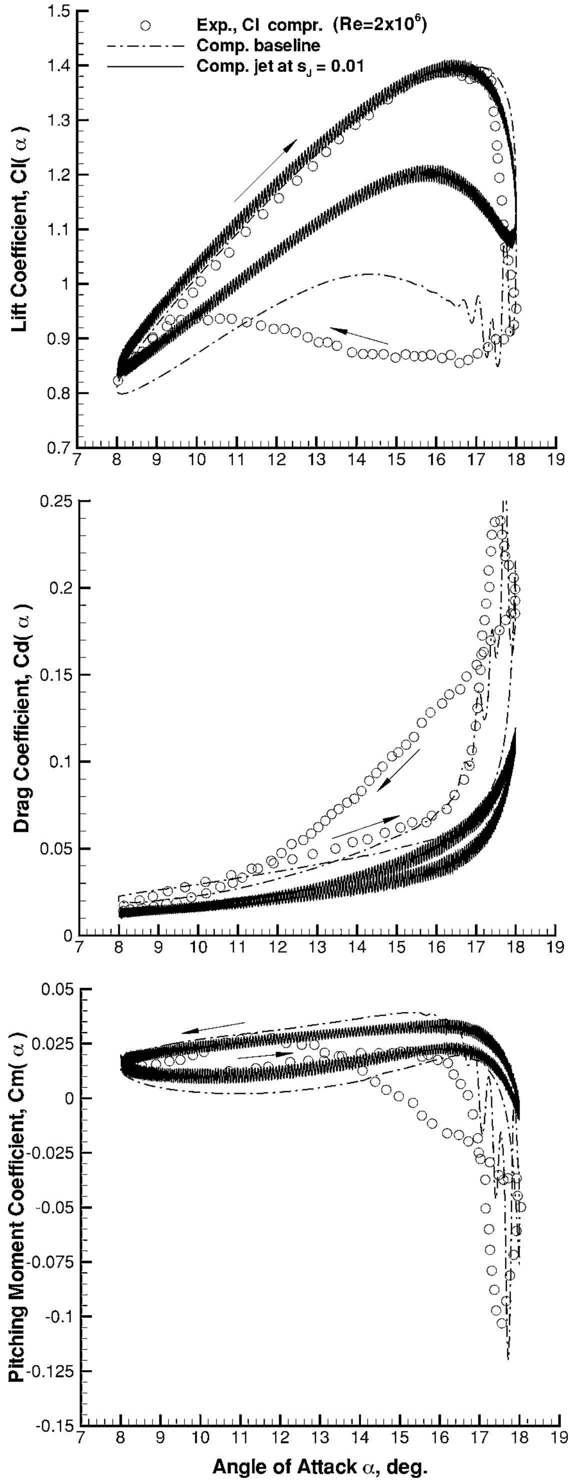

Fig. 5 Effect of pulsating jet flow control on the computed loads; $Re_c = 5.0 \times 10^6$ (fully turbulent incompressible), $\alpha(t) = 13$ deg + 5 $\sin(\omega_a t)$, $k_a = 0.05$ and $s_J = 0.1$, $F_J^+ = 6.3$, $C_\mu = 2.5\%$.

oscillation of the computed loads during the oscillation cycle is at the pulsation frequency of the jet.

The computed load hysteresis loop for flow control obtained by a pulsating jet located at $s_J = 0.1$ with $F^+ = 6.3$ and $C_\mu = 2.5\%$ is compared in Fig. 5 with the high-Reynolds-number measurements of Ref. 23 and the baseline airfoil computation. The higher pulsation level jet ($C_\mu = 2.5\%$) reduces the dynamic stall hysteresis effects effectively but causes an additional oscillation of the loads at the jet pulsation frequency and with a larger amplitude than the lower output level ($C_\mu = 0.5\%$) leading-edge jet of the preceding case. Significant reductions of the maximum excursions of the drag $Cd(\alpha)$ and pitching moment $Cm(\alpha)$ coefficients are observed.

The computed load hysteresis loop for flow control obtained by a a pulsating jet located at $s_J = 0.7$ with $F^+ = 6.3$ and $C_\mu = 2.5\%$ is compared in Fig. 6 with the high-Reynolds-number measurements of Ref. 23 and the baseline airfoil computation. It appears that dynamic stall has been effectively suppressed, and for qualitative comparison the measured lift hysteresis loop of Ref. 5 is shown in the same figure. The computed drag and pitching moment show insignificant hysteresis effects.

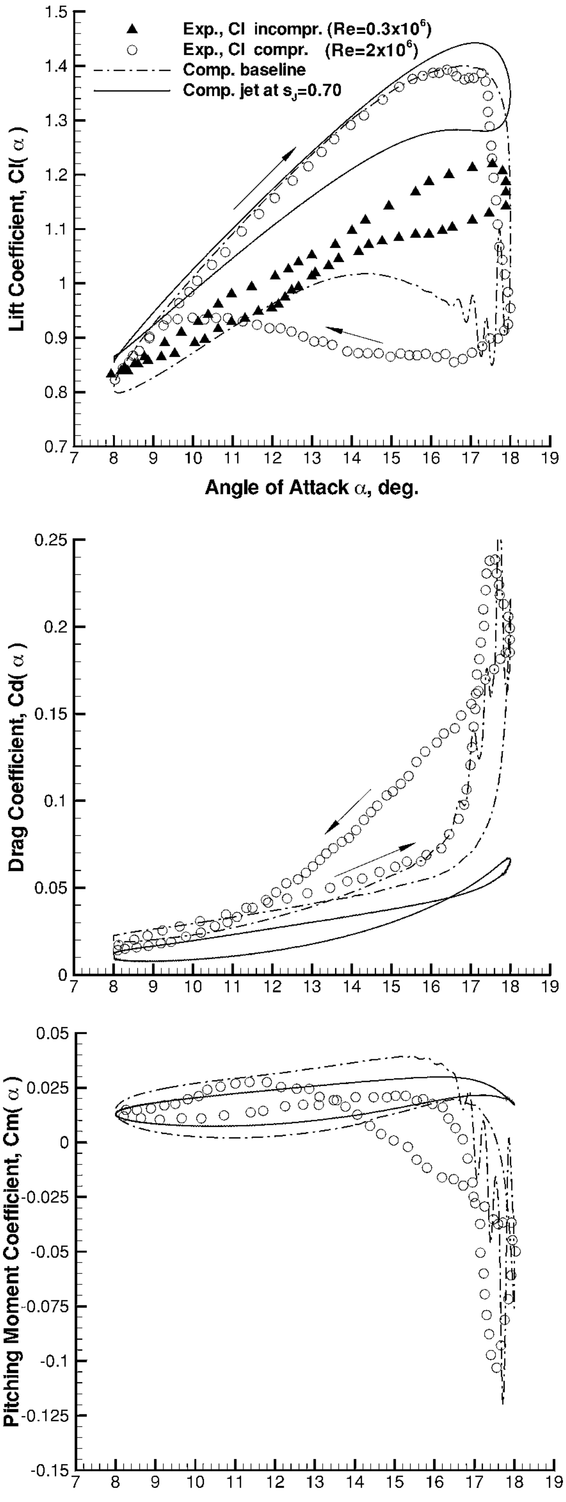

Fig. 6 Effect of pulsating jet flow control on the computed loads; $Re_c = 5.0 \times 10^6$ (fully turbulent incompressible), $\alpha(t) = 13$ deg + 5 sin$(\omega_a t)$, $k_a = 0.05$ and $s_J = 0.7$, $F_J^+ = 6.3$, $C_\mu = 2.5\%$.

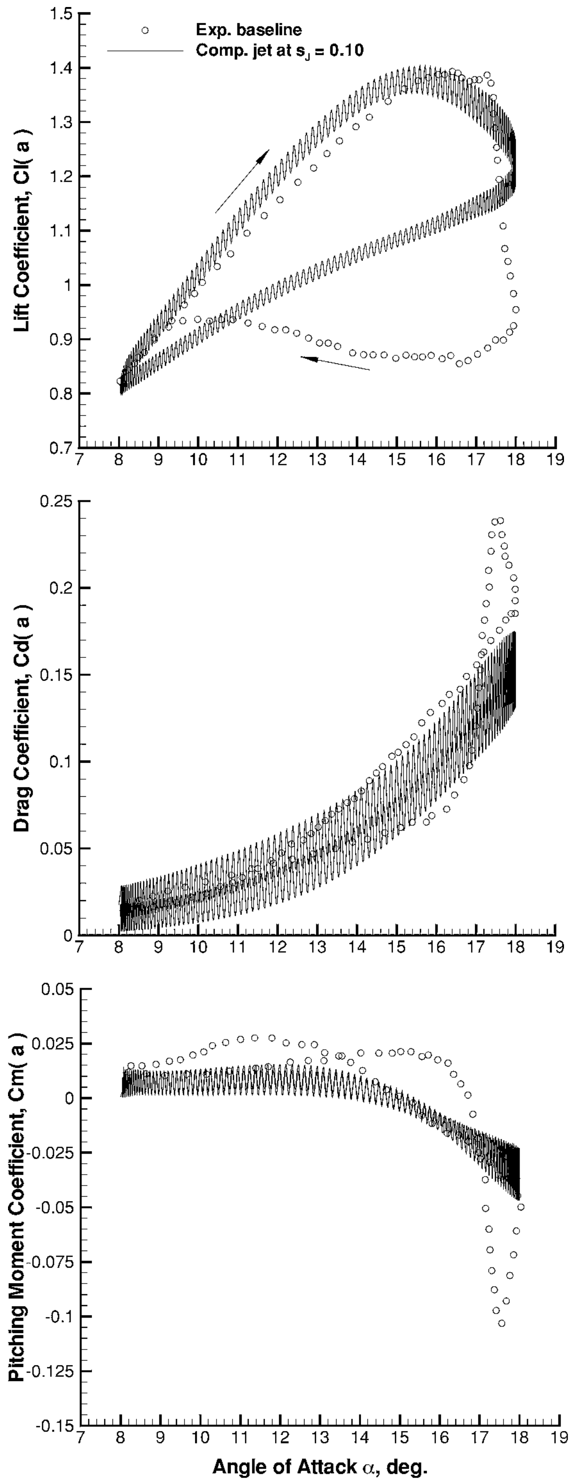

Fig. 7 Effect of pulsating jet flow control on the computed loads; $M_\infty = 0.3$, $Re_c = 5.0 \times 10^6$ (fully turbulent), $\alpha(t) = 13$ deg + 5 sin$(\omega_a t)$, $k_a = 0.05$ and $s_J = 0.1$, $F_J^+ = 3.1$, $C_\mu = 2.5\%$.

C. Compressible Flow Control

The computed load hysteresis loop for control of compressible flow dynamic stall, obtained by a pulsating jet located at $s_J = 0.1$ with $F^+ = 3.1$ and $C_\mu = 2.5\%$, is compared in Fig. 7 with the high-Reynolds-number measurements of Ref. 23. The high pulsation level of the jet $C_\mu = 2.5\%$ reduces the dynamic stall hysteresis effects effectively but causes a significant oscillation of the loads at the jet pulsation frequency. A lower jet pulsation frequency $F^+ = 3.1$ was chosen for the control of compressible flows. As a result, the reductions of the maximum excursions of the drag $Cd(\alpha)$ and pitching-moment $Cm(\alpha)$ coefficients are not as large as in the incompressible flow case. Numerical experiments with pulsating jet flow control for fixed angles of incidence indicated that for certain angles of incidence and jet locations addition of a steady component to the zero mass oscillating jet can have beneficial effects. It is seen, however, in Fig. 8 that flow control of dynamic stall with a pulsating jet, which generates the same momentum coefficient C_μ as the zero net mass flow pulsating jet of the preceding case but has a steady component ($V_0 > 0$), is not effective. The computed excursions for flow control with a nonzero net mass flux pulsating jet, shown

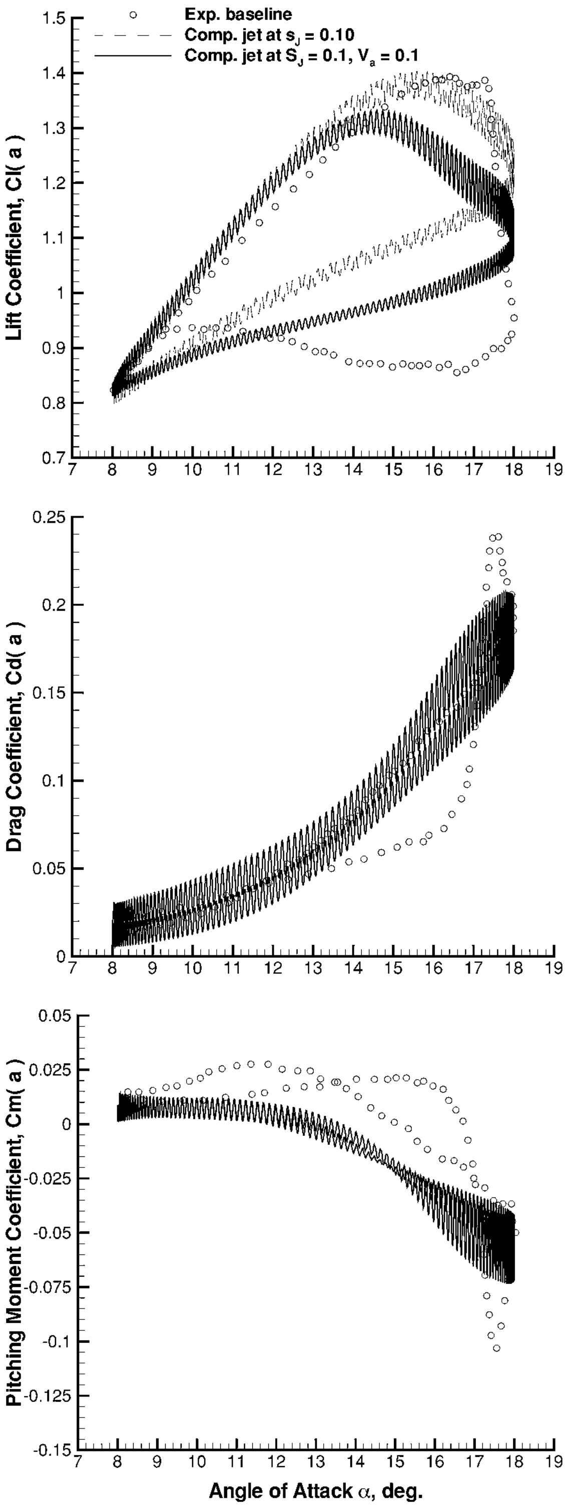

Fig. 8 Effect nonzero mean ($V_0 = 0.1$) on the computed loads; $M_\infty = 0.3$, $Re_c = 5.0 \times 10^6$ (fully turbulent), $\alpha(t) = 13\ \text{deg} + 5\sin(\omega_a t)$, $k_a = 0.05$ and $s_J = 0.1$, $F_J^+ = 3.1$, $C_\mu = 2.5\%$.

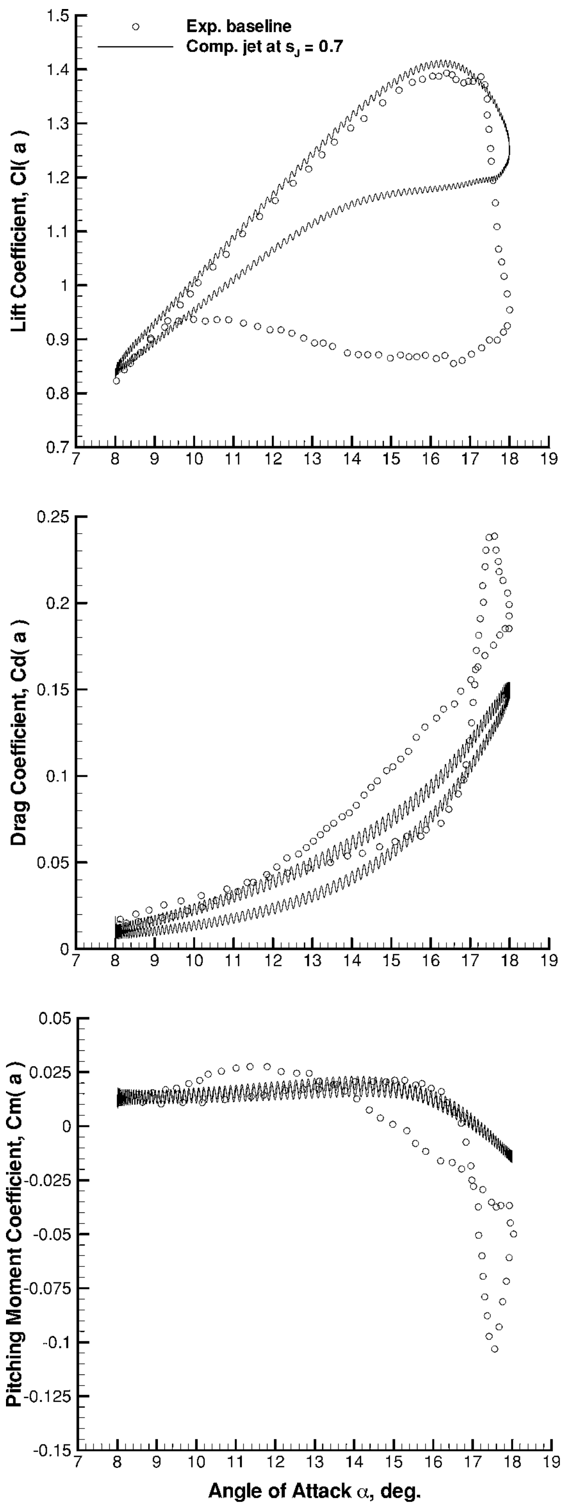

Fig. 9 Effect of pulsating jet flow control on the computed loads; $M_\infty = 0.3$, $Re_c = 5.0 \times 10^6$ (fully turbulent), $\alpha(t) = 13\ \text{deg} + 5\sin(\omega_a t)$, $k_a = 0.05$ and $s_J = 0.7$, $F_J^+ = 3.1$, $C_\mu = 2.5\%$.

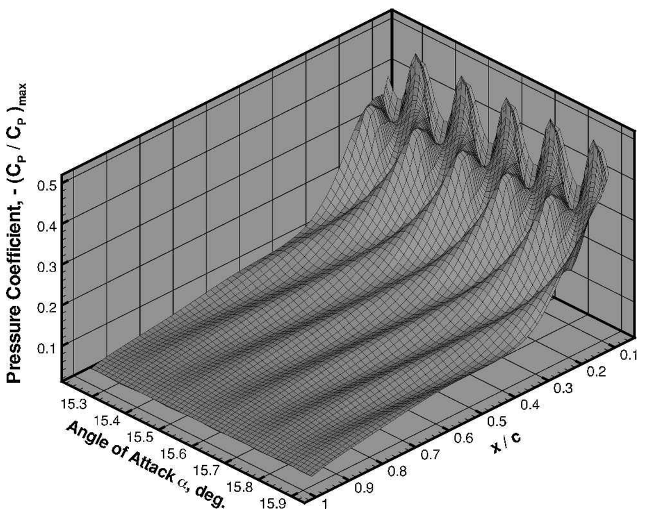

Fig. 10 Variation of the computed surface pressure coefficient caused by pulsating jet flow control at $s_J = 0.10$.

in Fig. 8, have the same order of magnitude as the uncontrolled flow.

Finally, the computed load hysteresis loop for control of compressible flow dynamic stall obtained by a pulsating jet located at $s_J = 0.7$ with $F^+ = 3.1$ and $C_\mu = 2.5\%$ is compared in Fig. 9 with the high-Reynolds-number measurements of Ref. 23. The high output of the jet ($C_\mu = 2.5\%$) reduces the dynamic stall hysteresis effects effectively and for the location $s_J = 0.7$ causes a small oscillation of the loads at the jet pulsation frequency. The reductions of the maximum excursions of the drag $Cd(\alpha)$ and pitching-moment $Cm(\alpha)$ coefficients are significant as in the incompressible flow case.

It has been observed in experiments[2] that pulsating jets generate coherent structures that propagate downstream and energize the boundary layer. The coherent structures generated by a pulsating jet at 10% chord can be clearly seen in Fig. 10, where the surface-pressure coefficient during several cycles of pulsation is plotted vs angle of incidence.

V. Conclusions

Numerical simulations of pulsating jet flow control for a NACA-0015 airfoil were carried out. Time-accurate solutions of the RANS equations with a one-equation turbulence model were used. The pulsating jet flow control was simulated by imposing a harmonically varying transpiration boundary condition on the airfoil surface. It was found that effective flow control can be achieved for the time-dependent flow over the harmonically oscillating airfoil, which if uncontrolled leads to development of deep stall. Both incompressible and compressible high-Reynolds-number flow was considered. The effect of control parameters such as jet location and exit angle, momentum coefficient C_μ, and pulsation frequency F^+ were considered in both incompressible and compressible flow investigations. For both incompressible and compressible flow the best location of the pulsating jet for most effective suppression of deep dynamic stall was predicted at the 70% chord location.

References

[1] Chang, R. C., Hsiao, F. B., and Shyu, R. N., "Forcing Level Effects of Internal Acoustic Excitation on the Improvement of Airfoil Performance," *AIAA Journal*, Vol. 29, No. 5, 1992, pp. 823–829.

[2] Greenblatt, D., Nishiri, B., Dabari, A., and Wygnanski, I., "Some Factors Affecting Stall Control with Particular Emphasis on Dynamic Stall," AIAA Paper 99-3504, June 1999.

[3] Seifert, A., and Pack, L. G., "Oscillatory Control of Separation at High Reynolds Numbers," *AIAA Journal*, Vol. 37, No. 9, 1999, pp. 1062–1079.

[4] Weaver, D., McAllister, K. W., and Tso, J., "Suppression of Dynamic Stall by Steady and Pulsed Upper-Surface Blowing," AIAA Paper 98-2413, June 1998.

[5] Greenblatt, D., and Wygnanski, I., "Parameters Affecting Dynamic Stall Control by Oscillatory Excitation," AIAA Paper 99-3121, June 1999.

[6] Chandrasekhara, M. S., Wilder, M. C., and Carr, L. W., "Compressible Dynamic Stall Control Using a Shape Adaptive Airfoil," AIAA Paper 99-0650, Jan. 1999.

[7] Chandrasekhara, M. S., Wilder, M. C., and Carr, L. W., "Compressible Dynamic Stall Control: A Comparison of Different Approaches," AIAA Paper 99-3122, June 1999.

[8] Rao, J. L., Ko, G. J., Strganac, T., and Rediniotis, O. K., "Flow Separation Control via Synthetic Jet Actuation," AIAA Paper 2000-0407, Jan. 2000.

[9] McCormick, D. C., "Boundary Layer Separation Control with Directed Synthetic Jets," AIAA Paper 2000-0519, Jan. 2000.

[10] Smith, B. L., and Glezer, A., "The Formation and Evolution of Synthetic Jets," *Physics of Fluids*, Vol. 10, No. 9, 1988, pp. 2281–2297.

[11] Gad-el-Hak, M., and Bushnell, D. M., "Separation Control: Review," *Journal of Fluids Engineering*, Vol. 113, No. 5, 1991, pp. 5–30.

[12] Ekaterinaris, J. A., and Platzer, M. F., "Computational Prediction of Dynamic Stall," *Progress in Aerospace Sciences*, Vol. 33, No. 11–12, 1997, pp. 759–846.

[13] Geissler, W., and Sobieczky, H., "Unsteady Flow Control on Rotor Airfoils," AIAA Paper 95-0189, Jan. 1995.

[14] Wu, J. M., Lu, X. Y., and Wu, J. Z., "Post-Stall Lift Enhancement on an Airfoil by Local Unsteady Control, Part II. Mode Competition and Vortex Dynamics," AIAA Paper 97-2046, June 1997.

[15] Ravindran, S. S., "Active Control of Flow Separation over an Airfoil," NASA TM-1999-209838, 1999.

[16] Hassan, A. A., and JanakiRam, R. D., "Effects of Zero-Mass Synthetic Jets on the Aerodynamics of the NACA-0012 Airfoil," AIAA Paper 97-2326, June 1997.

[17] Hassan, A. A., "Numerical Simulations and Potential Applications of Zero-Mass Jets for Enhanced Rotor Aerodynamic Performance," AIAA Paper 98-0211, Jan. 1998.

[18] Donovan, J. F., Kral, L. D., and Cary, A. W., "Active Control Applied to an Airfoil," AIAA Paper 98-0210, Jan. 1998.

[19] Ekaterinaris, J. A., and Menter, F. R., "Computation of Oscillating Airfoil Flows with One- and Two-Equation Turbulence Models," *AIAA Journal*, Vol. 32, No. 12, 1994, pp. 2359–2365.

[20] Ekaterinaris, J. A., "Numerical Investigation of Dynamic Stall of an Oscillating Wing," *AIAA Journal*, Vol. 33, No. 10, 1995, pp. 1803–1808.

[21] Ekaterinaris, J. A., Chandrasekhara, M. S., and Platzer, M. F., "Analysis of Low Reynolds Number Airfoils," *Journal of Aircraft*, Vol. 32, No. 3, 1995, pp. 625–630.

[22] Ekaterinaris, J. A., Sorensen, N. N., and Rasmussen, F., "Numerical Investigation of Airfoil Dynamic Stall in Simultaneous Oscillatory and Translational Motion," *Journal of Solar Energy Engineering*, Vol. 120, No. 2, Feb. 1998, pp. 75–83.

[23] Piziali, R. A., "2-D and 3-D Oscillating Wing Aerodynamics for a Range of Angles of Attack Including Stall," NASA-TM 4632, 1994; also USAATCOM TR 94-A-011, 1994.

[24] Chorin, A. J., "Numerical Methods for Solving Incompressible, Viscous Flow Problems," *Journal of Computational Physics*, Vol. 2, No. 1, 1967, pp. 12–26.

[25] Merkle, C. L., and Athavale, M., "Time-Accurate Unsteady Incompressible Flow Algorithm Based on Artificial Compressibility," AIAA Paper 87-1137, June 1987.

[26] Ekaterinaris, J. A., "Numerical Simulation of Incompressible Two-Blade Rotor Flowfields," *Journal of Propulsion and Power*, Vol. 14, No. 3, 1998, pp. 367–374.

[27] Rogers, S. E., Kwak, D., and Kiris, C., "Steady and Unsteady Solutions of the Incompressible Navier–Stokes Equations," *AIAA Journal*, Vol. 29, No. 4, 1991, pp. 603–610.

[28] Roe, P. L., "Approximate Riemann Solvers, Parameter Vectors, and Difference Schemes," *Journal of Computational Physics*, Vol. 43, No. 2, 1981, pp. 357–372.

[29] Spalart, P. R., and Allmaras, S. R., "A One-Equation Turbulence Model for Aerodynamic Flows," AIAA Paper 92-0439, Jan. 1992.

[30] Hassan, A. A., and Munts, E. A., "Transverse and Near-Tangent Synthetic Jets for Aerodynamic Flow Control," AIAA Paper 2000-4334, Aug. 2000.